Full band gap for surface acoustic waves in a piezoelectric phononic crystal

Vincent Laude, Mikaël Wilm, Sarah Benchabane, and Abdelkrim Khelif
Institut FEMTO-ST, département LPMO, CNRS UMR 6174, 32 avenue de l'Observatoire, F-25044 Besançon, France
(Received 16 November 2004; published 15 March 2005)

A plane-wave-expansion method suited to the analysis of surface-acoustic-wave propagation in two-dimensional piezoelectric phononic crystals is described. The surface modes of a square-lattice Y-cut lithium niobate phononic crystal with circular void inclusions with a filling fraction of 63% are identified. It is found that a large full band gap with a fractional bandwidth of 34% exists for surface acoustic waves of any polarization and incidence, coincidentally with the full band gap for bulk waves propagating in the plane of the surface. The excitation of surface acoustic waves by interdigital transducers is discussed.

DOI: 10.1103/PhysRevE.71.036607 PACS number(s): 46.40.Cd, 63.20.−e, 72.50.+b, 77.65.Dq

I. INTRODUCTION

Phononic crystals are periodic structures made of materials with different elastic properties [1,2]. They are receiving increasing attention as they enable the realization of perfect mirrors, the confinement of acoustic energy in defect modes, and the fabrication of very efficient waveguides. All these functions can be achieved in a very tight space of the order of some acoustic wavelengths. Phononic crystals are similar to photonic crystals but for the peculiarities of elastic as compared to optical waves. Among these, the propagation of elastic waves can be strongly anisotropic, various combinations of shear and longitudinal polarizations can exist, and surface modes almost always exist at the phononic crystal boundaries. Most studies of phononic crystals have focused on the propagation of bulk acoustic or elastic waves [3–11]. The consideration of bulk waves in phononic crystal experiments is analogous to the use of external light sources in photonic crystal experiments. Bulk elastic waves are generally generated outside the sample of interest—for instance, using acoustic transducers. However, surface acoustic waves (SAW's) can be conveniently excited at the surface of a piezoelectric solid and they are widely employed in ultrasonics, especially for high-frequency applications. For instance, SAW devices fabricated on piezoelectric materials such as quartz, lithium niobate, or lithium tantalate are extensively used as passive radio-frequency telecommunication filters [12]. The importance of surface waves in this context originates from their direct excitation and detection by interdigital transducers on the surface of piezoelectric materials [13].

Surface waves propagating at the surface of a two-dimensional Al-Hg phononic crystal have been observed by Torres *et al.* [14]. Plane-wave-expansion- (PWE-) based methods have been used to investigate the propagation of surface modes in two-dimensional phononic crystals with a solid-solid composition [15–17]. Tanaka and Tamura [15] obtained the dispersion relations of surface modes for phononic crystals consisting of circular cylinders of AlAs forming a square lattice in a GaAs matrix. They observed the existence and gave the stop band distribution of true surface (Rayleigh) and pseudosurface modes (leaky modes). They later reported similar findings for phononic crystals consisting of aluminum cylinders forming a triangular lattice in a polymer matrix [16]. This study was subsequently generalized by Wu *et al.* [17] to solid-solid elastic compositions with general anisotropy.

Here we focus on surface-acoustic-wave propagation in piezoelectric phononic crystals and their band gaps. For definiteness, we consider the case of lithium niobate ($LiNbO_3$) as the piezoelectric material in numerical simulations, though the mathematical derivations in this paper are valid for an arbitrary piezoelectric material. The propagation of bulk and surface waves in a piezoelectric material is necessarily anisotropic. Furthermore, an electromagnetic wave accompanies the elastic wave along its propagation. Accordingly, we use and extend a PWE method suited to piezocomposite materials [18]. The phononic crystals we consider are two dimensional in nature; they are composed of a periodic repetition of hollow cylinders inside a solid matrix, with the cylinders axes normal to the propagation surface, as depicted in Fig. 1. The solid-vacuum composition is interesting for applications since it optimizes the contrast between the matrix and scatterer properties. The hollow cylinders might in practice be realized by microtechniques or nanotechniques—for instance, using reactive ion etching (RIE) and focused ion beam (FIB) milling. With such techniques, solid-vacuum compositions are generally easier to obtain than solid-solid compositions involving the subsequent filling of holes in the solid matrix with a different material.

Following the traditional approach for piezoelectric materials, the existence of surface modes is revealed by the vanishing of the free and shorted boundary condition determinants for a plane and homogeneous surface. These boundary conditions are here generalized to the case of a periodically structured surface. The concepts of a Green's dyadic and of an effective permittivity matrix (EPM) are further introduced, again generalizing traditional SAW procedures. The density of surface states is also computed and used to predict the band structure of surface modes. The procedure is illustrated with the Y cut of lithium niobate, and the existence of a wide full band gap for surface modes is found. We observe the existence of many surface modes which do not exist on an homogeneous surface and are a consequence of the periodic structuration of the surface.

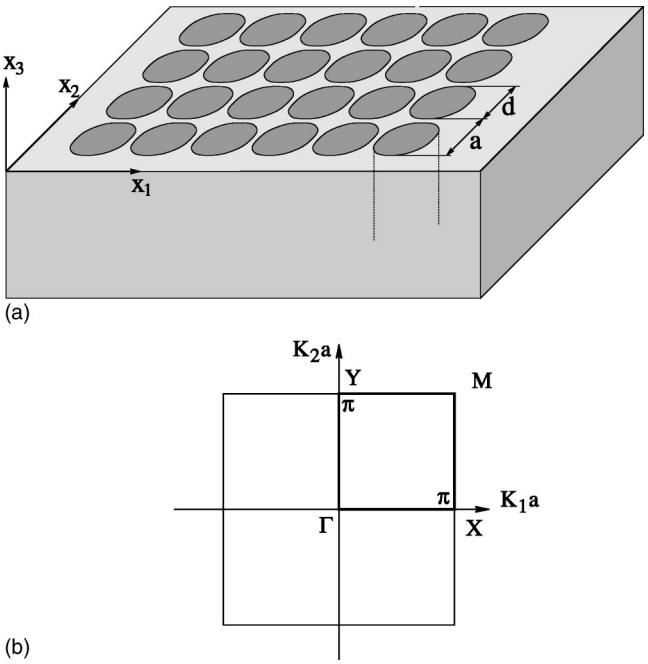

FIG. 1. (a) Square-lattice two-dimensional phononic crystal consisting of cylindrical holes in a Y-cut lithium niobate substrate ($d=0.9a$) and (b) the corresponding first irreducible Brillouin zone.

II. PLANE-WAVE-EXPANSION THEORY

Sections II A and II B are essentially a summary of the PWE method originally exposed in Ref. [18] in the context of piezocomposite materials. Sections II C and II D are extensions of the theory to the representation of holes in a phononic crystal and to the problem of identifying surface modes, respectively.

A. PWE basics

According to the Bloch-Floquet theorem, all fields in a periodic solid, such as displacements or stresses, can be expanded as an infinite series:

$$h(\boldsymbol{r},t)=\sum_{\boldsymbol{G}} h_{\boldsymbol{G}}(\omega,\boldsymbol{k})\exp\left[j(\omega t-\boldsymbol{k}\cdot\boldsymbol{r}-\boldsymbol{G}\cdot\boldsymbol{r})\right], \tag{1}$$

where $\boldsymbol{r}=(x_1,x_2,x_3)^T$ and the vectors of the reciprocal lattice are $\boldsymbol{G}=(2\pi m_1/a_1,2\pi m_2/a_2,0)^T$. In this expression, $\boldsymbol{k}$ is the Bloch-Floquet wave vector and h stands for either the displacements u_i, the stresses T_{ij}, the electric potential ϕ, or the electric displacements D_i, with $i,j=1,2,3$.

The periodicity of the structure is also used to expand the material constants as a Fourier series:

$$\alpha(\boldsymbol{r})=\sum_{\boldsymbol{G}} \alpha_{\boldsymbol{G}} e^{-j\boldsymbol{G}\cdot\boldsymbol{r}}, \tag{2}$$

where α is either one of ρ, c_{ijkl}, e_{ijk}, or ϵ_{ij}, with $i,j,k,l=1,2,3$. ρ is the material density, and c_{ijkl}, e_{ijk}, and ϵ_{ij} are the elastic, piezoelectric, and dielectric tensors, respectively. The Fourier harmonics $\alpha_{\boldsymbol{G}}$ are easily calculated for various scatterers and lattice geometries [17,19].

It is useful to define a generalized displacement field $\tilde{\boldsymbol{u}}$ in which $\tilde{u}_4$ represents the electric potential ϕ, and generalized stress vectors $\tilde{\boldsymbol{t}}_i=(T_{i1},T_{i2},T_{i3},D_i)^T$. We further group the generalized displacements and the generalized stresses normal to the surface in the eight-component state vector $\tilde{\boldsymbol{h}}=(\tilde{\boldsymbol{u}},\tilde{\boldsymbol{t}}_3)^T$. Assuming a truncation to a total of N harmonics in the two-dimensional Fourier expansions, the following vector notations are considered for the harmonics of the generalized stress and displacement fields ($4N$ components each):

$$\tilde{\boldsymbol{T}}_i=(\tilde{\boldsymbol{t}}_{i\boldsymbol{G}_1}\cdots\tilde{\boldsymbol{t}}_{i\boldsymbol{G}_N})^T, \tag{3}$$

$$\tilde{\boldsymbol{U}}=(\tilde{\boldsymbol{u}}_{\boldsymbol{G}_1}\cdots\tilde{\boldsymbol{u}}_{\boldsymbol{G}_N})^T, \tag{4}$$

where the vectors of the reciprocal lattice, $\boldsymbol{G}_m$, are labeled using a single index m.

Bulk waves are obtained as the eigensolutions of the secular equation

$$\omega^2\tilde{R}\tilde{\boldsymbol{U}}=\sum_{i,l=1,3}\Gamma_i\tilde{A}_{il}\Gamma_l\tilde{\boldsymbol{U}}, \tag{5}$$

with the $4N\times4N$ matrices Γ_i, $\tilde{A}_{il}$ and $\tilde{R}$ defined by the $N\times N$ blocks with 4×4 elements

$$(\Gamma_i)_{mn}=\delta_{mn}(k_i+G_{im})I_4, \tag{6}$$

$$(\tilde{A}_{il})_{mn}=A_{il\boldsymbol{G}_m-\boldsymbol{G}_n}, \tag{7}$$

$$(\tilde{R})_{mn}=\rho_{\boldsymbol{G}_m-\boldsymbol{G}_n}\tilde{I}_4, \tag{8}$$

with I_4 the 4×4 identity matrix, $\tilde{I}_4=I_4$ but for $\tilde{I}_4(4,4)=0$, and

$$A_{il\boldsymbol{G}}(j,k)=c_{ijkl\boldsymbol{G}},\quad A_{il\boldsymbol{G}}(j,4)=e_{lij\boldsymbol{G}},$$

$$A_{il\boldsymbol{G}}(4,k)=e_{ikl\boldsymbol{G}},\quad A_{il\boldsymbol{G}}(4,4)=-\epsilon_{il\boldsymbol{G}}, \tag{9}$$

with $i,j,k,l=1,2,3$ and $m,n=1,\ldots,N$. Equation (5) defines a generalized eigenvalue problem which can be solved for ω^2 as a function of $\boldsymbol{k}$ to obtain the band structure of bulk waves.

The two-dimensional phononic crystal of Fig. 1 is not periodic along the x_3 axis and k_3 can be obtained as a function of the other parameters of the model—i.e., k_1, k_2, and ω—as the eigenvalue of the equation

$$\begin{bmatrix}\omega^2\tilde{R}-B & 0\\ -C_2 & I_d\end{bmatrix}\tilde{\boldsymbol{H}}=k_3\begin{bmatrix}C_1 & I_d\\ D & 0\end{bmatrix}\tilde{\boldsymbol{H}}, \tag{10}$$

where the eigenvector is $\tilde{\boldsymbol{H}}=(\tilde{\boldsymbol{U}},j\tilde{\boldsymbol{T}}_3)^T$ and with

$$B=\sum_{i,j=1,2}\Gamma_i\tilde{A}_{ij}\Gamma_j,\quad C_1=\sum_{i=1,2}\Gamma_i\tilde{A}_{i3},$$

$$C_2=\sum_{j=1,2}\tilde{A}_{3j}\Gamma_j,\quad D=\tilde{A}_{33}. \tag{11}$$

Solving this system yields $8N$ complex-valued eigenvalues k_{3q} and eigenvectors $\tilde{\boldsymbol{H}}_q$. By grouping in the eigenvectors the eight components corresponding to the mth harmonic, we introduce the notation

$$\tilde{\boldsymbol{h}}_{mq} = \begin{pmatrix} (u_i)_{\boldsymbol{G}_m q} \\ \phi_{\boldsymbol{G}_m q} \\ (T_{3j})_{\boldsymbol{G}_m q} \\ (D_3)_{\boldsymbol{G}_m q} \end{pmatrix}, \tag{12}$$

with $i,j=1,2,3$, $m=1,\ldots,N$, and $q=1,\ldots,8N$. The generalized displacement and normal stress fields are obtained from the superposition with relative amplitudes A_q:

$$\tilde{\boldsymbol{h}}(\boldsymbol{r},t) = \sum_{m=1}^{N} \sum_{q=1}^{8N} A_q \tilde{\boldsymbol{h}}_{mq} \exp\{j[\omega t - (\boldsymbol{G}_m + \boldsymbol{k}_q)\cdot \boldsymbol{r}]\}. \tag{13}$$

This superposition is a finite approximation to the infinite series (1). Each individual term $\tilde{\boldsymbol{H}}_q \exp[j(\omega t - \boldsymbol{k}_q \cdot \boldsymbol{r})]$ in the superposition is termed a partial wave in the following.

B. Surface boundary conditions

Since we consider a semi-infinite (though composite) substrate, only physically valid partial waves must be included in the normal mode expansion (13). Due to the tensor symmetries of the material constants and for real-valued k_1 and k_2, the partial waves belong in pairs to an ensemble of $4N$ slowness curves. Hence, for each partial wave, using a criterion based on the sign of the component of the time-averaged Poynting vector that is normal to the surface [20] (in the case of a propagative partial wave) or on the sign of the imaginary part of k_{3q} (in the case of an evanescent partial wave), an unambiguous modal selection can be performed. We are then left with exactly $4N$ partial waves describing waves in the interior of the substrate. The eigenvectors $\tilde{\boldsymbol{H}}_q$ can then be restricted to the selected $4N$ partial waves.

The boundary conditions for surface modes apply at the $x_3=0$ surface. The mechanical boundary conditions require the nullity of stress components normal to the surface or

$$\sum_{q=1}^{4N} A_q (T_{3j})_{\boldsymbol{G}_m q} = 0, \tag{14}$$

for a total of $3N$ conditions. In the derivation of boundary conditions, the orthogonality of the $\exp(j\boldsymbol{G}_m \cdot \boldsymbol{r})$ harmonic functions over one period of the surface is used [18]. From the electrical point of view, the free and shorted boundary conditions are considered. The free boundary condition is that the component of the electric displacement normal to the surface is continuous, resulting in

$$\sum_{q=1}^{4N} A_q [(D_3)_{\boldsymbol{G}_m q} - \epsilon_0 |\kappa_m| \phi_{\boldsymbol{G}_m q}] = 0, \tag{15}$$

with $|\kappa_m| = \sqrt{(k_1+G_{1m})^2 + (k_2+G_{2m})^2}$ and with ϵ_0 the permittivity of vacuum. The shorted boundary condition considers that the electric potential at the surface vanishes—for instance, because of the presence of a thin perfectly conducting metallic layer—yielding

$$\sum_{q=1}^{4N} A_q \phi_{\boldsymbol{G}_m q} = 0. \tag{16}$$

Both electrical boundary conditions result in a total of N conditions.

C. Solid-void phononic crystals

The PWE method summarized in Secs. II A and II B assumes implicitly a solid-solid composition. In order to describe also solid-void compositions, the material constants of one of the two solids must be modified. More precisely, this modification must be such that the interfaces between the solid matrix (solid 1) and the inclusions (solid 2) are free of tractions. We first let the piezoelectric constants in solid 2 vanish and impose $\epsilon_{ij}^{(2)} = \epsilon_0$. The equations of motion in solid 2 are then purely elastic:

$$T_{ij}^{(2)} = \sum_{k,l=1}^{3} c_{ijkl}^{(2)} \frac{\partial u_k^{(2)}}{\partial x_l}, \tag{17}$$

$$\rho^{(2)} \frac{\partial^2 u_j^{(2)}}{\partial t^2} = \sum_{i=1}^{3} \frac{\partial T_{ij}^{(2)}}{\partial x_i}. \tag{18}$$

Since there are no stresses in a vacuum, we set $c_{ijkl}^{(2)}=0$ to impose $T_{ij}^{(2)}=0$ independently of the displacements, which are precisely defined in solid 2 only at the interfaces. As a consequence, we set $\rho^{(2)}=0$ or otherwise from Eq. (18) the displacements at the interface would not be free.

Conversely, is the solution above compatible with the conditions defining a free interface? The relations of continuity at the interface between two solids are $u_i^{(1)}=u_i^{(2)}$ and $\Sigma_{j=1}^3 T_{ij}^{(1)} n_j = \Sigma_{j=1}^3 T_{ij}^{(2)} n_j$, where n_j defines the outward normal. At a free interface, the displacements $u_i^{(1)}$ are unspecified and $\Sigma_{j=1}^3 T_{ij}^{(1)} n_j = 0$. Clearly both sets of conditions are compatible if $c_{ijkl}^{(2)}=0$ and $\rho^{(2)}=0$ simultaneously. We have thus defined a simple pseudosolid that will fake a vacuum in solid-solid PWE computations. It is worth pointing out that no numerical instabilities result, since the Fourier coefficients in Eq. (2) are still well defined, though using the material constants of only one solid.

D. Surface modes

In the case of a shorted surface, the surface boundary conditions (14) and (16) must be satisfied simultaneously. This yields a system of $4N$ linear equations in the $4N$ unknown amplitudes A_q, which has a nontrivial solution only if the determinant

$$\Delta_s(\omega, k_1, k_2) = \begin{vmatrix} (T_{3j})_{\boldsymbol{G}_m q} \\ \phi_{\boldsymbol{G}_m q} \end{vmatrix} \tag{19}$$

vanishes. Thus the SAW solutions on a shorted surface can be identified by locating the zeros of Δ_s. Similarly, in the case of a free surface, the SAW solutions can be identified by locating the zeros of the determinant

$$\Delta_f(\omega,k_1,k_2) = \begin{vmatrix} (T_{3j})_{\boldsymbol{G}_m q} \\ (D_3)_{\boldsymbol{G}_m q} \end{vmatrix}, \tag{20}$$

where we have made the substitution

$$(D_3)_{\boldsymbol{G}_m q} \leftarrow (D_3)_{\boldsymbol{G}_m q} - \epsilon_0 |\kappa_m| \phi_{\boldsymbol{G}_m q}. \tag{21}$$

This substitution is assumed from now on. As in the case of a homogeneous substrate, it can be expected that a simultaneous zero of both determinants Δ_s and Δ_f is the signature of a nonpiezoelectrically coupled surface mode. Indeed, in this case, the surface mode is insensitive to the electrical boundary conditions. Conversely, in the case there exists a (small) frequency shift between two zeros of the determinants, this shift can be used to obtain an estimate of the piezoelectric coupling factor K^2 of the surface mode, according to the usual formula $K^2 = 2(\omega_f - \omega_s)/(\omega_f + \omega_s)$.

A surface Green's dyadic (generalizing the surface Green's dyadic or Green's function of the homogeneous piezoelectric substrate) can be obtained by eliminating the partial waves amplitudes from Eq. (13). At the surface, we take the scalar product over one period of the surface of Eq. (13), restricted to the $4N$ selected partial waves, with the N harmonic functions $\exp(j\boldsymbol{G}_m \cdot \boldsymbol{r})$ or

$$\begin{aligned} &\frac{1}{a_1 a_2} \int \tilde{\boldsymbol{h}}(\boldsymbol{r},t) \exp(j\boldsymbol{G}_m \cdot \boldsymbol{r}) d\boldsymbol{r} \\ &\quad = \sum_{q=1}^{8N} A_q \tilde{\boldsymbol{h}}_{mq} \exp(j(\omega t - k_1 x_1 - k_2 x_2) \\ &\quad = \tilde{\boldsymbol{h}}_m \exp(j(\omega t - k_1 x_1 - k_2 x_2) \ . \end{aligned} \tag{22}$$

Upon defining the $8N$-component vector

$$\tilde{\boldsymbol{H}} = (\tilde{\boldsymbol{h}}_1 \ldots \tilde{\boldsymbol{h}}_N)^T = \begin{pmatrix} (u_i)_{\boldsymbol{G}_m} \\ \phi_{\boldsymbol{G}_m} \\ (T_{3j})_{\boldsymbol{G}_m} \\ (D_3)_{\boldsymbol{G}_m} \end{pmatrix}, \tag{23}$$

we have the vector-matrix relation between the harmonics of the generalized displacements and generalized stresses:

$$\begin{pmatrix} (u_i)_{\boldsymbol{G}_m} \\ \phi_{\boldsymbol{G}_m} \end{pmatrix} = G \times \begin{pmatrix} (T_{3j})_{\boldsymbol{G}_m} \\ (D_3)_{\boldsymbol{G}_m} \end{pmatrix}, \tag{24}$$

with the Green's dyadic

$$G = \begin{pmatrix} u_{i\boldsymbol{G}_m q} \\ \phi_{\boldsymbol{G}_m q} \end{pmatrix}^{-1} \times \begin{pmatrix} (T_{3j})_{\boldsymbol{G}_m q} \\ D_{3\boldsymbol{G}_m q} \end{pmatrix}. \tag{25}$$

The Green's dyadic is a $4N \times 4N$ square matrix and relates the generalized displacements to the generalized stresses. This is a direct generalization of the 4×4 Green's dyadic of a homogeneous piezoelectric semi-infinite substrate.

The concept of an effective permittivity for surface acoustic waves on an homogeneous substrate is very useful [21]. Such an effective permittivity is a scalar function relating the normal electric displacement to the potential of a plane-wave solution with a given wave vector and frequency, in the case of a mechanically free surface. In the case treated here, there are N Fourier harmonics which have to be considered for every wave vector and frequency couple. Then an effective permittivity matrix $\boldsymbol{\epsilon}_{\text{eff}}$ can be defined by relating the normal electric displacement harmonics to the potential harmonics—i.e., $[(D_3)_{\boldsymbol{G}_m}] = \boldsymbol{\epsilon}_{\text{eff}}[\phi_{\boldsymbol{G}_m}]$. Using the boundary condition (14), we obtain at once that the effective permittivity matrix is given by the lower right $N \times N$ submatrix of the inverse Green's dyadic.

Before closing this section, we define two useful scalar functions for locating surface modes. First, we remark that in the case of a homogeneous substrate, the effective permittivity is proportional to the function $b(\omega,k_1,k_2) = \Delta_f/\Delta_s$. This property is not valid anymore for a piezocomposite material as considered here. However, this function still gives direct information on piezoelectrically coupled surface modes, since its poles indicate surface modes on the shorted surface while its zeros indicate surface modes on a free surface. Second, we can define the variation of the total density of surface states according to the formula [22]

$$\Delta n(\omega,k_1,k_2) = \frac{1}{\pi} \operatorname{Im}\left\{ \frac{\partial}{\partial \omega} \ln|G| \right\}. \tag{26}$$

This function is zero when there are no surface modes and presents poles where there are.

III. RESULTS

In this section, we exemplify the PWE theory in the case of the square-lattice lithium-niobate phononic crystal depicted in Fig. 1. For a Y-cut substrate, the crystallographic axis Y is the outward normal to the surface, which is also the XZ plane. The reference frame used for the PWE method is chosen to be $(x_1,x_2,x_3) = (X,-Z,Y)$. Lithium niobate belongs to the trigonal $3m$ crystallographic class so that the XY plane is a symmetry plane. Propagation in the plane of the surface along axes Z and $-Z$ is then equivalent. The holes have a circular cross section with a diameter $d = 0.9a$, where a is the lattice constant. The filling fraction $\pi^2 d^2/(4a^2)$ then equals 63%. Seven harmonics are used in each direction in the PWE computations, resulting in a total of $N = 49$ harmonics. By increasing this number, it was verified that computations, and especially band structures, are within 1%-precision for all presented results.

It is first instructive to consider the bulk and surface acoustic waves propagating in the plane of the surface of a homogeneous (i.e., without holes) substrate of lithium niobate, as depicted in Fig. 2. The propagation of piezoelastic waves is clearly anisotropic with relatively large velocity variations. In addition to the longitudinal and the two shear bulk elastic modes, there exists two kind of surface modes on the homogeneous surface. The Rayleigh SAW is a true (lossless) surface mode located in the subsonic region—i.e., at velocities lower than that of all bulk waves. This SAW is

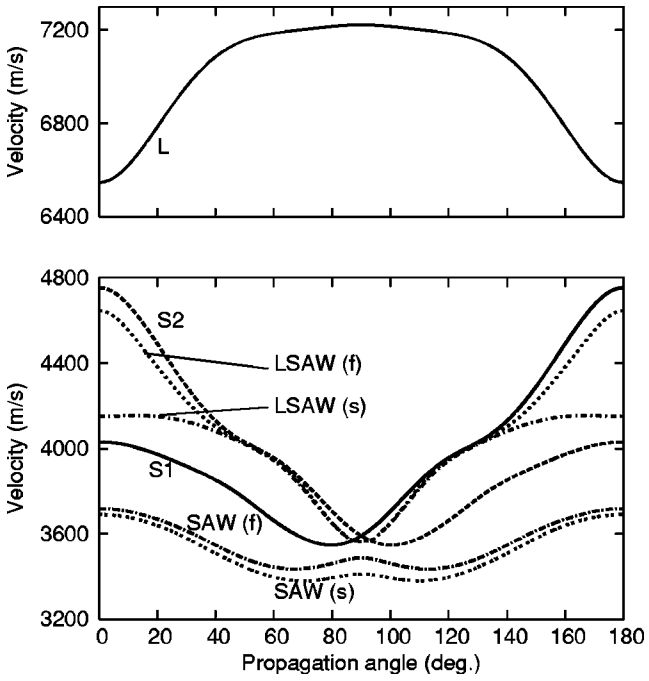

FIG. 2. Velocities of bulk and surface modes in the *XZ* plane of Y-cut lithium niobate, as a function of the propagation angle. The longitudinal (L) and shear (S1 and S2) bulk acoustic waves are shown. The Rayleigh surface acoustic wave (SAW) and the leaky surface acoustic wave (LSAW) are shown for free (f) and shorted (s) electrical boundary conditions.

sensitive to the electrical surface boundary condition for all propagation angles. The difference in the free and shorted velocities is a direct measure of the piezoelectric coupling coefficient of this wave. The leaky SAW (LSAW) is a lossy surface mode located mostly in the hypersonic region—i.e., at velocities in between that of the two shear bulk waves. The LSAW is also very sensitive to the electrical surface boundary condition. Its piezoelectric coupling coefficient is maximum in the *X* direction but vanishes in a wide angular range about the *Z* direction—i.e., from 40° to 140°.

Figure 3 displays the band structure for bulk waves propagating in the plane of the phononic crystal, plotted along the closed path Γ-*X*-*M*-*Y*-Γ in the first irreducible Brillouin zone [Fig. 1(b)]. Due to the lattice symmetry and to the anisotropy of lithium niobate, this path is the shortest yielding comprehensive information on band gaps. It can be seen that a full band gap (i.e., a band gap for any direction of propagation and polarization) exists for bulk waves propagating in plane from $\omega a/(2\pi)=1935$ m/s to 2745 m/s. The fractional bandwith is then larger than 34%. Qualitatively, it can be observed that although in principle anisotropy makes it more difficult to open a full band gap than with isotropic materials, the free boundaries of void inclusions are very efficient scatterers for elastic waves of any polarization. The frequency width of the band gap is defined solely by the *M* point.

Figure 4 displays the variations of the free and shorted boundary condition determinants of Eqs. (19) and (20) as a function of frequency, for the *X* and *M* points of the first irreducible Brillouin zone. The occurrence of surface modes

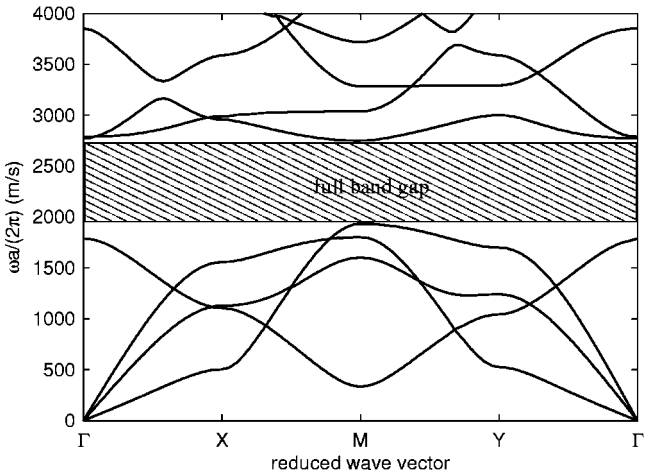

FIG. 3. Band structure along the path Γ-*X*-*M*-*Y*-Γ in the first irreducible Brillouin zone for bulk waves propagating in the plane of the phononic crystal of Fig. 1 (i.e., with $k_3=0$).

is indicated by zeros (or sharp minima in the case of leaky modes). As a general rule, it can be observed that there exist many surface modes in the phononic crystal, both below and above the full band gap for bulk waves, but not within it. This multiplicity of surface modes was not mentionned in the

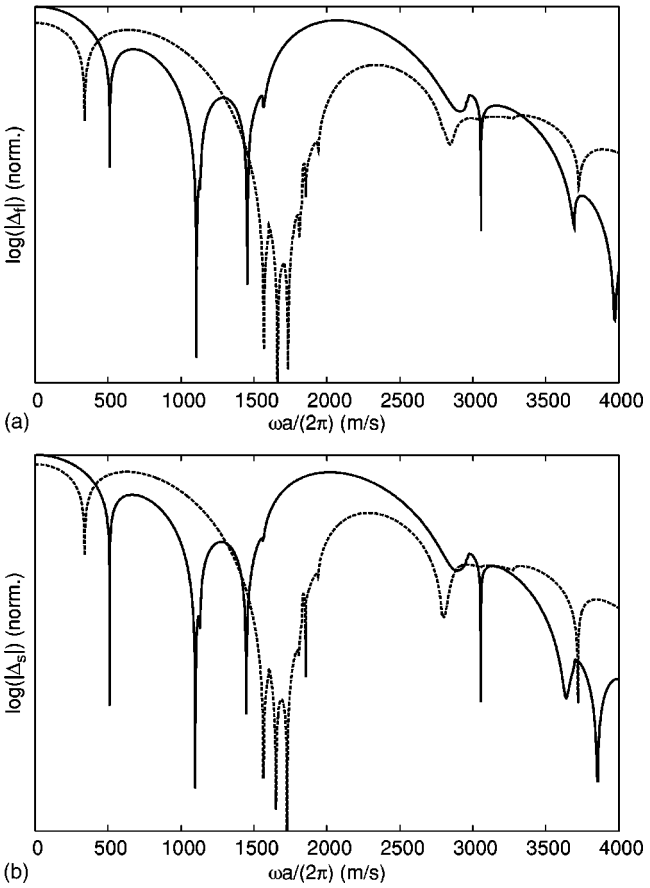

FIG. 4. Free (a) and shorted (b) boundary conditions determinants for the *X* (solid line) and *M* (dotted line) points of the first irreducible Brillouin zone, for the lithium niobate phononic crystal of Fig. 1.

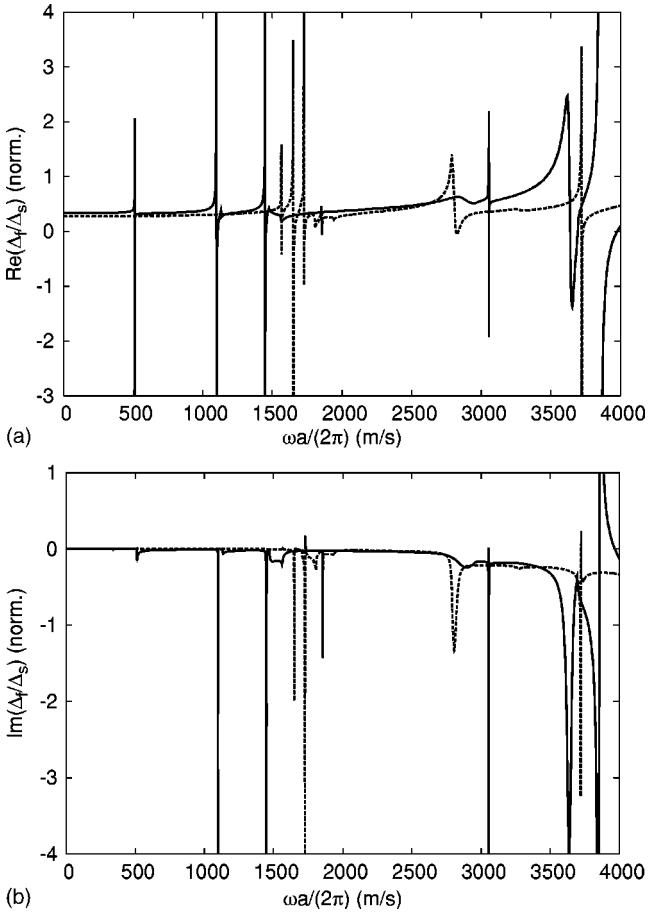

FIG. 5. Real (a) and imaginary (b) parts of the free and shorted boundary conditions determinants ratio for the X (solid line) and M (dotted line) points of the first irreducible Brillouin zone, for the lithium niobate phononic crystal of Fig. 1.

case of the solid-solid phononic crystals of Refs. [15–17], but is clearly apparent in previous studies of surface modes in superlattices [22,23], which can be viewed as one-dimensional phononic crystals. The contributions of bulk waves can also be seen in the form of discontinuities of the first derivative of the determinants. The ratio of the two boundary condition determinants is shown in Fig. 5. Poles of this function indicate the existence of piezoelectrically coupled surface modes, since for uncoupled surface modes the two determinants have identical zeros that compensate one another.

Figure 6 shows the band structure for surface modes along the path Γ-X-M-Y-Γ. This band structure clearly has similarities with the band structure of bulk waves propagating in the plane of the surface of Fig. 3. This plot is obtained using the modulus of the variation of the total density of surface states, Eq. (26). The surface mode branches define a full band gap that is exactly coincident with that for in-plane propagating bulk waves. This result is not obvious since the $4N$ partial waves defining a surface mode include evanescent waves as well as bulk waves propagating obliquely in the phononic crystal, with possibly any direction and polarization state. We observe that surface mode branches often exist just below bulk branches, as in the case of the homogeneous

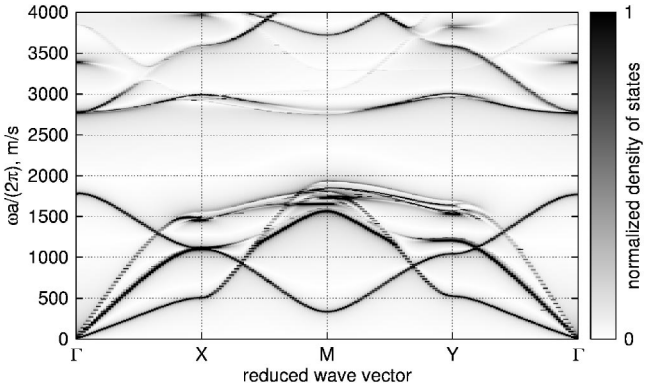

FIG. 6. Band structure for surface modes along the path Γ-X-M-Y-Γ in the first irreducible Brillouin zone, for the lithium niobate phononic crystal of Fig. 1.

substrate, but not exclusively. In addition to the existence of a full band gap, which offers the basis for phononic crystal functions in combination with usual interdigital transducers, such as mirrors, waveguides, or filters, the variety of surface modes in phononic crystals is also interesting in itself. However, we do not attempt here to identify the details of these surface modes—e.g., their attenuation, coupling, and dispersion.

As already pointed out, a distinctive advantage of considering a piezoelectric material is the possibility to generate and detect surface modes using usual interdigital transducers (IDT's) directly inside or in close proximity to the phononic crystal. For instance, assuming a simple transducer with an alternate potential of +1 and −1 V applied to the IDT fingers, the resonance condition for SAW generation and detection is

$$\frac{\omega p}{2\pi} = \frac{v}{2}, \tag{27}$$

with p the transducer pitch and v the SAW velocity. This relation in combination with the band structure of Fig. 6 makes it possible to design an IDT for frequencies inside the full band gap. For instance, if the phononic crystal has a lattice constant $a = 1$ μm, then the full band gap extends approximately from 1.95 to 2.75 GHz. For an IDT pitch $p = 0.85$ μm, it can be verified from Fig. 2 that the Rayleigh SAW and the LSAW on the homogeneous surface are simultaneously within the full band gap for any propagation direction.

IV. CONCLUSION

A plane-wave-expansion method suited to the analysis of surface-acoustic-wave propagation in phononic crystals has been described. The surface modes of a square-lattice phononic crystal made of Y-cut lithium niobate with void circular inclusions have been obtained. A full band gap for surface waves with a fractional bandwidth of 34% has been found, coincidentally with the full band gap for bulk waves

propagating in the plane of the surface. We conjecture that this property generally applies to all phononic crystals, although it is at present only the result of a numerical observation. We suspect that it is directly related to the existence of band gaps for bulk elastic waves propagating out of plane [9], since these obliquely propagating bulk waves contribute to the plane-wave expansion of the surface modes. However, the analysis presented in Ref. [9] would need to be extended to all complex branches of the band structure, whereas it was limited to only the real branches.

ACKNOWLEDGMENT

We gratefully acknowledge support in this work from the Action Concertée Nanosciences 2004 (Project No. NR137).

[1] M. M. Sigalas and E. N. Economou, Solid State Commun. **86**, 141 (1993).
[2] M. S. Kushwaha, P. Halevi, L. Dobrzynski, and B. Djafari-Rouhani, Phys. Rev. Lett. **71**, 2022 (1993).
[3] J. V. Sanchez-Perez, D. Caballero, R. Martinez-Sala, C. Rubio, J. Sanchez-Dehesa, F. Meseguer, J. Llinares, and F. Galves, Phys. Rev. Lett. **80**, 5325 (1998).
[4] F. R. Montero de Espinosa, E. Jimenez, and M. Torres, Phys. Rev. Lett. **80**, 1208 (1998).
[5] D. Caballero, J. Sanchez-Dehesa, C. Rubio, R. Martinez-Sala, J. V. Sanchez-Perez, F. Meseguer, and J. Llinares, Phys. Rev. E **60**, R6316 (1999).
[6] J. O. Vasseur, P. A. Deymier, B. Chenni, B. Djafari-Rouhani, L. Dobrzynski, and D. Prevost, Phys. Rev. Lett. **86**, 3012 (2001).
[7] T. Miyashita, Jpn. J. Appl. Phys., Part 1 **41**, 3170 (2002).
[8] A. Khelif, A. Choujaa, B. Djafari-Rouhani, M. Wilm, S. Ballandras, and V. Laude, Phys. Rev. B **68**, 214301 (2003).
[9] M. Wilm, A. Khelif, S. Ballandras, V. Laude, and B. Djafari-Rouhani, Phys. Rev. E **67**, 065602(R) (2003).
[10] A. Khelif, A. Choujaa, S. Benchabane, B. Djafari-Rouhani, and V. Laude, Appl. Phys. Lett. **84**, 4400 (2004).
[11] A. Khelif, M. Wilm, V. Laude, S. Ballandras, and B. Djafari-Rouhani, Phys. Rev. E **69**, 067601 (2004).
[12] K. Hashimoto, *Surface Acoustic Wave Devices in Telecommunications—Modelling and Simulation* (Springer, Berlin, 2000).
[13] R. M. White and F. W. Voltmer, Appl. Phys. Lett. **17**, 314 (1965).
[14] M. Torres, F. R. Montero de Espinosa, D. Garcia-Pablos, and N. Garcia, Phys. Rev. Lett. **82**, 3054 (1999).
[15] Y. Tanaka and S. I. Tamura, Phys. Rev. B **58**, 7958 (1998).
[16] Y. Tanaka and S. I. Tamura, Phys. Rev. B **60**, 13 294 (1999).
[17] T.-T. Wu, Z.-G. Huang, and S. Lin, Phys. Rev. B **69**, 094301 (2004).
[18] M. Wilm, S. Ballandras, V. Laude, and T. Pastureaud, J. Acoust. Soc. Am. **112**, 943 (2002).
[19] J. O. Vasseur, B. Djafari-Rouhani, L. Dobrzynski, M. S. Kushwaha, and P. Halevi, J. Phys.: Condens. Matter **6**, 8759 (1994).
[20] R. Peach, IEEE Trans. Ultrason. Ferroelectr. Freq. Control **48**, 1308 (2001).
[21] K. A. Ingebrigtsen, J. Appl. Phys. **40**, 2681 (1969).
[22] E. H. El Boudouti, B. Djafari-Rouhani, E. M. Khourdifi, and L. Dobrzynski, Phys. Rev. B **48**, 10 987 (1993).
[23] E. H. El Boudouti, B. Djafari-Rouhani, and A. Nougaoui, Phys. Rev. B **51**, 13 801 (1995).